

**THREE-DIMENSIONAL WIND FIELD CONSTRUCTION, WIND
TURBINE CITING AND WIND COMFORT ANALYSIS IN AN URBAN
ENVIRONMENT**

by

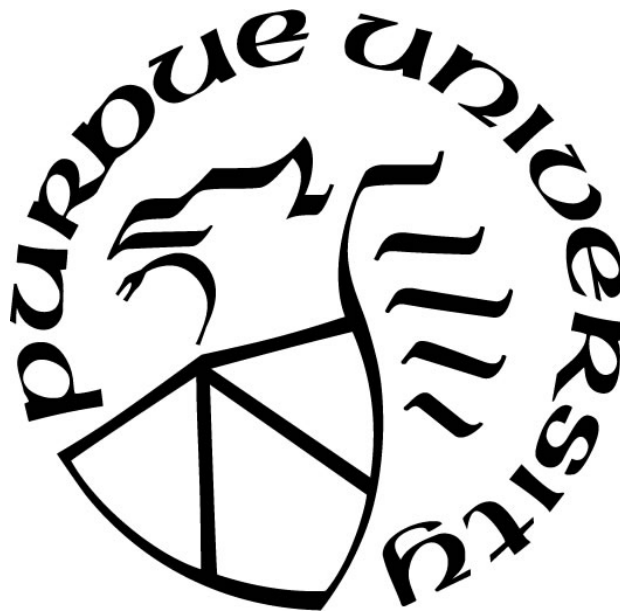
Mingrui Liu

A Thesis

Submitted to the Faculty of Purdue University

In Partial Fulfillment of the Requirements for the degree of

Master of Science in Mechanical Engineering



Department of Mechanical and Civil Engineering

Hammond, Indiana

December 2020

THE PURDUE UNIVERSITY GRADUATE SCHOOL
STATEMENT OF COMMITTEE APPROVAL

Dr. Xiuling Wang, Chair

Department of Mechanical and Civil Engineering

Dr. Masoud Mojtahed

Department of Mechanical and Civil Engineering

Dr. Ran Zhou

Department of Mechanical and Civil Engineering

Approved by:

Dr. Chenn Zhou

ACKNOWLEDGEMENTS

Here is a great opportunity to express my gratitude to my advisor, Dr. Xiuling Wang, for her time, patience and effort for mentoring me. She provided many valuable research skills and valuable suggestions to give me a direction for my current and future research and career.

Then, I would like to thank all staff and faculty in the department of Mechanical and Civil Engineering in Purdue Northwest. They are always prepared to answer various questions and work as a competitive team. All the courses I took in the past years helped me a lot when I did this research. I also want to thank Professors Masoud Mojtahed and Ran Zhou for serving as the examining committee.

TABLE OF CONTENTS

LIST OF TABLES	6
LIST OF FIGURES	7
NOMENCLATURE	9
ABSTRACT.....	10
1. INTRODUCTION	11
1.1 Background and Motivation	11
1.2 Literature Review.....	13
1.3 Objectives	15
2. METHODOLOGY AND METHODS	17
2.1 Pre-processing.....	17
2.2 Turbulence Models	17
2.3 Wind Inflow Condition.....	20
3. MODEL VALIDATION WITH WIND TUNNEL EXPERIMENT.....	22
3.1 One Building Case	22
3.1.1 Geometry and Mesh for One Building	22
3.1.2 Boundary Conditions.....	23
3.1.3 Comparison of Simulation Results for Various Turbulence Models with Wind Tunnel Testing Data	23
3.2 Two Buildings Case.....	26
3.2.1 Geometry and Mesh for Two Buildings Case	26
3.2.2 Boundary Conditions.....	27
3.2.3 Comparison of Simulation Results for Various Turbulence Models with Wind Tunnel Testing Data	27
3.3 Wind in A Dense Urban.....	29
3.3.1 Geometry and Mesh for A Dense Urban	29
3.3.2 Boundary Conditions.....	31
3.3.3 Comparison of Simulation Results for Various Turbulence Models with Wind Tunnel Testing Data	32
4. 3-D WIND FIELD CONSTRUCTION	35

4.1	Geometry of PNW Campus Buildings.....	35
4.2	Mesh Generation.....	39
4.3	Boundary Conditions	40
5.	URBAN WIND FLOW ANALYSIS	41
5.1	3-D Wind Field Simulation Results for Wind Turbine Citing.....	41
5.2	The Wind Comfort Analysis at Pedestrian Level	45
6.	CONCLUSIONS AND FUTURE WORK.....	50
	REFERENCES	52

LIST OF TABLES

Table 1. Boundary conditions	23
Table 2. The comparison between different turbulent models for single building case	26
Table 3. The comparison between different turbulent models for two buildings case	29
Table 4. Boundary conditions	32
Table 5. The comparison between different turbulent models for building density case	34
Table 6. Boundary conditions	40
Table 7. Eddy GT wind turbine properties and specifications.....	44

LIST OF FIGURES

Figure 1. Configuration for single building wind flow validation case	22
Figure 2. Computational mesh for single building case	24
Figure 3. Flow field around the building	25
Figure 4. Comparison of simulation results for various turbulence models and wind tunnel testing data.....	25
Figure 5. Configuration for two buildings wind flow validation case.....	26
Figure 6. Computational mesh for two buildings case	27
Figure 7. Flow field around the building	28
Figure 8. Comparison of simulation results for various turbulence models and wind tunnel testing data.....	28
Figure 9. Configuration for a dense urban wind flow validation case.....	30
Figure 10. Computational mesh for dense urban case	32
Figure 11. Flow field around the building	33
Figure 12. Comparison of simulation results for RSM turbulence model and wind tunnel testing data.....	33
Figure 13. Overview of the Purdue University Northwest (PNW) campus buildings.....	35
Figure 14. Location of three wind data sensors	36
Figure 15. 3-D model at different view of building layout.....	36
Figure 16. Overhead view of SULB	37
Figure 17. 3-D Gyte building model at different view	37
Figure 18. 3-D Porter Hall model at different view	37
Figure 19. 3-D Potterand Power building model at different view.....	38
Figure 20. 3-D CLO building model at different view	38
Figure 21. 3-D Anderson building model at different view.....	38
Figure 22. Mesh detail: mesh detail of SULB and surrounding buildings	39
Figure 23. Contour of wind velocity at height level 21m.....	41
Figure 24. Contour of wind velocity around SUL Building	42
Figure 25. Wind turbine installation location	43
Figure 26. Eddy GT Wind Turbine power output curve.....	44

Figure 27. Contour of wind velocity at height of 2m from ground	46
Figure 28. Wind velocity vector at height of 2m from ground.....	46
Figure 29. Wind velocity at pedestrian level along with sidewalk.....	48

NOMENCLATURE

ρ	Density
α	Power law exponent
ε	Turbulent kinetic energy dissipation rate
σ_k	Turbulence Prandtl number for k , 1.00
σ_ε	Turbulence Prandtl number for ε , 1.30
μ_t	Turbulent viscosity
μ	Viscosity
B	Building width
C_μ	k- ε turbulence model constant 0.09
$C_{1\varepsilon}$	k- ε turbulence model constant, 1.44
$C_{2\varepsilon}$	k- ε turbulence model constant, 1.92
G_k	Generation of turbulence kinetic energy due to the mean velocity gradients
G_b	Generation of turbulence kinetic energy due to buoyancy only when gravity and temperature gradient is present simultaneously
H	Building height
k	Turbulent kinetic energy
L	Building length
P	Pressure
t	Time
u_i	Velocity component
U	Velocity at the height of z
U_0	Reference velocity at the reference height Z_0
Z	Vertical distance from the surface
Z_0	Reference height

ABSTRACT

Three-dimensional urban wind field construction plays an important role not only in the analysis of pedestrian levels of comfort but also in the effectiveness of harnessing wind energy in an urban environment. However, it is challenging to accurately simulate urban wind flow due to the complex land use in urban environments. In this study, a three-dimensional numerical model was developed for urban wind flow construction. To obtain an accurate urban wind field, various turbulence models, including the Reynolds Stress Model (RSM), Shear-Stress Transport (SST) $k-\omega$, realizable $k-\varepsilon$, and Re-Normalization Group (RNG) $k-\varepsilon$ models were tested. Simulation results were compared with experimental data in the literature. The RSM model showed promising potential in simulating urban wind flow. The model was then adopted to simulate urban wind flow for Purdue University Northwest, which is located in the Northwest Indiana urban region. Based on the simulation results, the optimal location was identified for urban wind turbine siting and the wind comfort was analyzed in the walk sides between the buildings.

Keywords: three-dimensional wind field construction; urban wind environment; urban wind turbine siting; wind comfort analysis

1. INTRODUCTION

1.1 Background and Motivation

The existing energy crisis has made people pay more attention to renewable energy, which is a partial alternative to fossil energy [1]. Renewable energy provided an estimated about 11% of global final energy consumption in 2018, and had a slight increase from 9.6% in 2013 [2]. Wind is a natural phenomenon caused by air movement, and it is caused by solar radiant heat. Due to the rotation of the earth, the large-scale movement of the air is severely affected by Coriolis force [3]. Wind power capacity increased over 20% more than any other renewable technology in 2011 [4]. The wind drives the blades to rotate and converts wind energy into mechanical energy. Then through the conversion of gears, the internal impeller is driven to rotate for mechanical energy transmission. The impeller is located in a magnetic field. After rotating, it cuts the magnetic lines of induction to convert mechanical energy into electrical energy. In settling the wind turbine farm, there are two key points: the first is to choose the location to set up the wind turbine, and the second thing is to select the type of wind turbine. After determining these two things, it will become easy to start to install the wind turbine to get cleaning and renewable energy.

For the first part of choosing the location to install the wind turbine farm, determining the suitable installation location is principal. The shape of the building and the shape of the atmospheric boundary layer (ABL) are the two main factors that affect the behavior of the wind above the roof of the building [5]. The horizontal wind speed changes with the ground height (vertical wind shear) are an important parameter to characterize wind resources. However, this change in wind speed will be affected by obstacles such as buildings in urban areas. When the wind blows over these obstacles, the vertical wind shear will change.

Establishing a 3D wind field is a common method for evaluating wind energy through CFD technique. The CFD technique estimates the potential of wind energy by applying a large number of advanced calculation techniques and combining some experimental data. The Reynolds-averaged Navier-Stokes (RANS) or Large-eddy simulation (LES) can be utilized to

solve the full resolution of the turbulent flow equations at the atmospheric boundary layer [6]. With the help of CFD, many researchers have been done to observe the wind distribution among dense urban area and analyze the impact on pedestrians now. There are some cases that use CFD to study the distribution of wind around pedestrian height in actual buildings [7, 8]. However, calculation conditions are not consummate, for example, the boundary conditions, and the size of the threshold. Some guidelines on the application of industrial CFD, which explains the verification and approach of CFD results, have been published to clarify the approach of how to validate and verification CFD results [9-11]. These verification methods have been determined to be quite effective for the application of wind distribution around buildings. Some teams used various kinds of CFD codes to conduct wind tunnel experiments and the wind tunnel results with actual measurement results on site for comparative calculations. This method has been used to study the effects of various calculation parameters in different environments. The common feature of these research results is that they have conducted cross-experimentally comparisons under a great number of different parameters.

The standard k-epsilon turbulence model is a fundamental equation to simulate wind engineering and it is still used in the CFD simulation of wind energy right now. However, this turbulence model cannot give the accurate results of wind conditions in suburban and urban areas [12]. To solve this problem, CFD has other different turbulence models can be used in building density area cases. The realizable k-epsilon model improves quantitatively the discomfort estimation compared to the standard k-epsilon model. The RNG k- ϵ model is derived from strict statistical techniques. It is very close to the standard k- ϵ model, but the RNG model adds a new different condition to the epsilon (ϵ) equation, effectively improving the accuracy, and considering the turbulent eddies, so the accuracy in this part is improved [29]. The standard k- ϵ turbulence model is a high Reynolds number model. The RNG k- ϵ turbulence model provides an analytical formula that considers the flow viscosity of low Reynolds numbers. The function of these formulas depends on the correct treatment of the adjacent wall area, and these characteristics make the RNG k- ϵ turbulence model more reliable and accurate than the standard k- ϵ model in a wider range of flows. Since the realizable k- ϵ turbulence model with swirl correction is a newly emerging model, there is no clear evidence to show that it performs better than the RNG k- ϵ model. However, the preliminary research shows that the realizable k- ϵ model has a good result

on the flow separation and complex secondary flow in all $k-\epsilon$ models. Reynolds-stress Model (RSM) is a relatively complete classical turbulence model, with a high level of turbulence closure. This model can explain the complex conditions in turbulence and the influence of Reynolds stress.

1.2 Literature Review

Three-dimensional urban wind field construction is important for many activities: weather forecasting, natural ventilation system design, pedestrian comfort level analysis, atmospheric dispersion assessments, and urban wind energy harnessing. However, it is challenging to accurately simulate urban wind flow due to complex land usage and terrain conditions, as well as the variety of building shapes, heights, densities, and layout configurations in urban environments. Stathopoulos et al. provided some views on the potential benefits and challenges in urban wind energy [13]; they reviewed the urban wind energy knowledge and discussed some current issues. Recent progress that was made in urban wind energy assessment was also addressed.

Many researchers focus on urban wind field construction and analysis. The straightforward methods are wind tunnel testing and field measurements [14–17]. Earlier wind tunnel tests were done by Wiren et al. [14], where they conducted experimental studies of wind velocities in passages between and through block-type building models with various types of layouts. Later, Tsang et al. [15] focused on wind tunnel studies of a pedestrian-level wind environment around tall buildings. More recently, Weerasuriya et al. [16] conducted wind tunnel studies to uncover the effects of twisted wind flows on pedestrian-level wind fields in an urban environment. Finally, Li et al. performed wind tunnel studies and tried to find the correlation between urban space quantification and pedestrian-level ventilation [17].

With the rapid development of computational resources and meshing techniques, increasingly more researchers have used computational fluid dynamics along with measured wind tunnel data to simulate and analyze wind flow in an urban environment. Many of the simulations were conducted by using Reynolds-averaged Navier–Stokes (RANS) models or the large-eddy simulation (LES) approach. Blocken et al. [18] reviewed wind-tunnel and computational fluid

dynamics (CFD) techniques to address their accuracy for wind comfort assessment. A comparison between the RANS model and LES for urban wind simulations was provided. Rodi used various $k-\epsilon$ models, Reynolds stress models, and LES models for urban wind simulations [19], where the results were compared with experimental data. The performance, cost, and potential of solving complex flow problems using those turbulence models were also compared. Rodi pointed out that the use of RANS calculations underestimated the turbulence fluctuations in general, while the use of LES gave better simulation details of the turbulence flow with the cost of a large increase in computing time. In the LES model, the unresolved small-scale turbulent motion was modeled, which was less influenced by the boundary conditions. Johnson and Hunter simulated urban wind flow using the $k-\epsilon$ model and revealed the broad flow features [20]. Compared with the wind tunnel experiments, a general agreement between the numerical results and experimental data was demonstrated. Willis investigated and tested the CFD validation guidelines in an urban wind simulation [21], while Song and He conducted a numerical simulation using an LES model when evaluating pedestrian wind flow [22]; in their studies, different geometry and wind conditions were adopted and simulation results were compared with wind tunnel experimental data.

Different variations of RANS models were widely used by many others for simulating urban wind flow: Santiago and Martilli used the standard $k-\epsilon$ model when simulating wind flow over a regular array of cubes [23]; Zheng et al. conducted the pedestrian-level wind environment study via wind tunnel tests and realizable $k-\epsilon$ simulations [24]; Gnatowska et al. used the realizable $k-\epsilon$ model to simulate flow fields in an urban environment, where the results were compared with Particle Image Velocimetry (PIV) data in a wind tunnel and a detailed description of the velocity field in the built-up environment was obtained [25]; Akashi et al. employed the RNG $k-\epsilon$ model to simulate the urban wind flow under different building layout effects [26]; Hu et al. applied the RNG $k-\epsilon$ model during a quantitative investigation of the building density effects on residential wind environments [27]; and Liu et al. used the RNG $k-\epsilon$ model to simulate the wind distribution in an urban community with a full-scale geometrical model coupled with a micro scale model [28].

Among these modeling works, LES simulations can reproduce more accurate details of the turbulence flow, but because of its large computational cost, most researchers choose to use a RANS model for urban wind flow simulations instead. In urban wind flow analysis, understanding the flow features within the passages is more important than capturing the detailed turbulence features near wall regions. The RANS models satisfy these requirements and are more computationally affordable than a LES. Reiter compared the standard $k-\varepsilon$ model, realizable $k-\varepsilon$ model, and RSM model in urban wind simulations [27], but some other popular RANS models, such as the RNG $k-\varepsilon$ model and Shear-Stress Transport (SST) $k-\omega$ model were not included. The comparisons between different RANS models for urban wind flow simulations are limited in the literature.

There are for three main parts to this paper. First, various popular RANS turbulence models, including the RNG $k-\varepsilon$ model, realizable $k-\varepsilon$ model, $k-\omega$ SST model, and RSM, were used to simulate wind flow in an urban environment. The simulation results were compared with wind tunnel experimental data. Among all those models, the RSM showed the most promising results for urban flow simulations, with the simulation results closely matching the experimental data. Second, wind turbine siting in an urban environment was investigated for Purdue University Northwest campus. By implementing the selected turbulence model coupled with a year-long wind data analysis, an optimal location was selected for a small vertical axis wind turbine (VAWT). Third, the wind comfort was analyzed in the pedestrian crossing between the buildings in PNW campus.

1.3 Objectives

The objective of this thesis project was to construct the 3-D wind fields in an urban area with the better turbulence model. The Reynolds-averaged Navier-Stokes equations were solved by the RNG k -epsilon model, realizable k -epsilon model, k -Omega SST model with turbulence and Reynolds-stress model of turbulence in commercial software ANSYS® Fluent 19.1 (Ansys Inc., Canonsburg, PA, USA). The simulation urban model of 3-D wind field, wind velocity distribution, wind profiles were obtained at Purdue University Northwest (PNW) campus. Based on simulation studies of four different turbulence models and boundary conditions, the impact of different turbulence models and boundary conditions is reasonably described, and then chose the

better conditions to simulate the urban wind fields. This study also considers the wind comfort felt by pedestrians when the wind flow passes through the passage between the buildings. Numerical results can provide useful information for wind assessment and wind turbine siting in an urban environment. The simulation results were validated by recorded wind data on the top-roof of Student Union & Library Building.

2. METHODOLOGY AND METHODS

Three parts are presented here: the validation study of the various turbulence models adopted for urban wind field simulations and the urban wind flow analysis, turbine siting for Purdue University Northwest, which is located in Northwestern Indiana, a suburban environment and wind comfort in campus area.

2.1 Pre-processing

The wind data were recorded by the three sensors on the roof of the Student Union and Library Building (SULB) penthouse. When considering the year-long wind direction distribution, the dominant wind direction was from West-northwest (WNW) to South-southeast (SSE). The second most frequent wind direction, west-southwest (WSW) with a wind speed magnitude at 3.17m/s, was applied as the input wind conditions for the following wind flow simulation.

2.2 Turbulence Models

The commercial software ANSYS® Fluent 19.1 was used for the 3D wind field construction simulations. Reynolds-averaged Navier–Stokes models (RANS models) were used to solve the transport equations of the airflow and simulate all turbulence scales. The RANS models are widely used in urban flow simulations because they yield relatively accurate simulation results and are computationally efficient compared with LES models [30]. In this study, various RANS models, including realizable k- ϵ , RNG k- ϵ , k- ω SST, and RSM, were implemented to solve the two validation cases. Brief descriptions of each turbulence model are listed below.

The compressible RANS equation for air can be written in the form of a Cartesian tensor using the summation convention:

$$\frac{\partial \rho}{\partial t} + \frac{\partial}{\partial x_i} (\rho u_i) = 0 \quad (1)$$

$$(\rho u_i) + \frac{\partial}{\partial x_j} (\rho u_i u_j) = -\frac{\partial p}{\partial x_i} + \frac{\partial \sigma_{ij}}{\partial x_j} + \frac{\partial}{\partial x_j} (-\rho u_i' u_j') \quad (2)$$

The k-ε models assume that the turbulence viscosity is linked to the turbulence kinetic energy and turbulent frequency via the relation:

$$\mu_t = \rho \frac{k}{\omega} \quad (3)$$

In this research, turbulence flow was modeled using the realizable k-ε model, RNG k-ε model, k-ω SST model, and Reynolds-stress model (RSM) for airflow to compute the turbulent kinetic energy (k) and the turbulent kinetic energy dissipation (ε).

The exact k-ε equations have many terms that have not yet been calculated. In order to facilitate understanding and calculations, the standard k-ε model was proposed by Launder and Spalding, which can be used as a basic method that is applied to engineering flow field calculations. The kinetic energy and turbulence dissipation rates in this model are described as:

$$\frac{\partial}{\partial t} (\rho k) + \frac{\partial}{\partial x_i} (\rho k u_i) = \frac{\partial}{\partial x_j} \left[\left(\mu + \frac{\mu_t}{\sigma_k} \right) \frac{\partial k}{\partial x_j} \right] + P_k + P_b + S_k - \rho \varepsilon - Y_M \quad (4)$$

and

$$\frac{\partial}{\partial t} (\rho \varepsilon) + \frac{\partial}{\partial x_i} (\rho \varepsilon u_i) = \frac{\partial}{\partial x_j} \left[\left(\mu + \frac{\mu_t}{\sigma_k} \right) \frac{\partial \varepsilon}{\partial x_j} \right] + C_{1\varepsilon} \frac{\varepsilon}{k} (G_k + C_{3\varepsilon} G_b) - C_{2\varepsilon} \rho \frac{\varepsilon^2}{k} + S_\varepsilon \quad (5)$$

where u_i is velocity component in corresponding direction, μ_t is the turbulent viscosity computed by k and ε as follows:

$$\mu_t = \rho C_\mu \frac{k^2}{\varepsilon} \quad (6)$$

where C_μ , $C_{1\varepsilon}$, $C_{2\varepsilon}$, σ_k , σ_ε are constants, which are 0.09, 1.44, 1.92, 1.00, 1.30 respectively.

The Realizable k-ε model adds a formula to turbulent viscosity and adds a new transport equation to the dissipation rate, the expressions of k and ε are:

$$\frac{\partial}{\partial t} (\rho k) + \frac{\partial}{\partial x_i} (\rho k u_i) = \frac{\partial}{\partial x_j} \left[\left(\mu + \frac{\mu_t}{\sigma_k} \right) \frac{\partial k}{\partial x_j} \right] + P_k + P_b + S_k - \rho \varepsilon - Y_M \quad (7)$$

and

$$\frac{\partial}{\partial t} (\rho \varepsilon) + \frac{\partial}{\partial x_j} (\rho \varepsilon u_j) = \frac{\partial}{\partial x_j} \left[\left(\mu + \frac{\mu_t}{\sigma_k} \right) \frac{\partial \varepsilon}{\partial x_j} \right] + \rho C_1 S_\varepsilon + \rho C_2 \frac{\varepsilon^2}{k + \sqrt{v\varepsilon}} + C_{1\varepsilon} \frac{\varepsilon}{k} + C_{3\varepsilon} G_b + S_\varepsilon \quad (8)$$

where

$$C_1 = \max \left[0.43, \frac{\eta}{\eta + 5} \right], \eta = S \frac{k}{\varepsilon}, S = \sqrt{2S_{ij}S_{ij}} \quad (9)$$

The RNG k- ε model was derived from a strict statistical mathematical technique to solve the problem for the effect of a smaller Reynolds number flow viscosity. The RNG and realizable k- ε models have shown significant improvements over the standard k- ε model in terms of the flow characteristics, including strong streamline curvature, vortex, and rotation [31]. The equations for k and ε are:

$$\frac{\partial}{\partial t}(\rho k) + \frac{\partial}{\partial x_i}(\rho k u_i) = \frac{\partial}{\partial x_j} \left[\left(\mu + \frac{\mu_t}{\sigma_k} \right) \frac{\partial k}{\partial x_j} \right] + P_k - \rho \varepsilon \quad (10)$$

and

$$\frac{\partial}{\partial t}(\rho \varepsilon) + \frac{\partial}{\partial x_i}(\rho \varepsilon u_i) = \frac{\partial}{\partial x_j} \left[\left(\mu + \frac{\mu_t}{\sigma_\varepsilon} \right) \frac{\partial \varepsilon}{\partial x_j} \right] + C_{1\varepsilon} \frac{\varepsilon}{k} P_k + C_{2\varepsilon}^* \frac{\varepsilon}{k} P_k \quad (11)$$

where

$$C_{2\varepsilon}^* = C_{2\varepsilon} + \frac{C_\mu \eta^3 (1 - \eta / \eta_0)}{1 + \beta \eta^3}, \quad \eta_0 = 4.38 \quad (12)$$

The Shear-Stress Transport (SST) k- ω model is a two-equation eddy-viscosity model. The inner parts of the boundary layer are solved using the k- ω model, while the k- ε model was implemented in the free shear flow. This model shows good behavior in adverse pressure gradients and separating flow regions. Menter [32] discussed this method in detail. The appropriate transport behavior can be obtained by formulating the vortex viscosity as follows:

$$v_t = \frac{a_1 k}{\max(a_1 \omega_r, SF_2)} \quad (13)$$

Note that the production term of ω is given by:

$$P_\omega = \left(\frac{a_3}{v_t} \right) \quad (14)$$

This formulation differs from the standard k- ε model. The kinetic energy and the specific dissipation rate equations are:

$$\frac{\partial k}{\partial t} + U_j \frac{\partial k}{\partial x_j} = \frac{\partial}{\partial x_j} \left[(v + \sigma_k v_T) \frac{\partial k}{\partial x_j} \right] + P_k - \beta^* k \omega \quad (15)$$

and

$$\frac{\partial \omega}{\partial t} + U_j \frac{\partial \omega}{\partial x_j} = \alpha S^2 - \beta \omega^2 + \frac{\partial}{\partial x_j} \left[(v + \sigma_\omega v_T) \frac{\partial \omega}{\partial x_j} \right] + 2(1 - F_1) \sigma_{\omega 2} \frac{1}{\omega} \frac{\partial k}{\partial x_j} \frac{\partial \omega}{\partial x_j} \quad (16)$$

Where

$$P_k = \min\left(\tau_{ij} \frac{\partial U_i}{\partial x_j}, 10\beta^* k\omega\right), F_1 = \tan \tanh \left\{ \min \left[\max \left(\frac{\sqrt{k}}{\beta^* \omega y}, \frac{500\nu}{y^2 \omega} \right), \frac{4\sigma_{\omega 2}}{CD_{k\omega y^2}} \right] \right\}^4 \quad (17)$$

The Reynolds stress model (RSM), known as the Reynolds stress transport model, represents the most complete classical turbulence model. The method of closure used is usually called a second-order closure. This model can explain the complex conditions in turbulent flow and the Reynolds stress's effects. The governing equations for the transport and momentum are written as follows:

$$\begin{aligned} \frac{\partial \rho \underline{U_i U_j}}{\partial t} + \frac{\partial k}{\partial x_k} (\underline{U_k \rho U_i U_j}) - \frac{\partial}{\partial x_k} \left[\left(\delta_{kl} \mu + \rho C_S \frac{k}{\varepsilon} \underline{U_k U_l} \right) \frac{\partial U_i U_j}{\partial x_l} \right] \\ = P_{ij} - \frac{2}{3} \delta_{ij} \rho \varepsilon + \phi_{ij} + P_{ij,b} \end{aligned} \quad (18)$$

and

$$\frac{\partial \rho U_i}{\partial t} + \frac{\partial}{\partial x_j} (\rho U_i U_j) - \frac{\partial}{\partial x_j} \left[\mu \left(\frac{\partial \rho U_i}{\partial x_j} + \frac{\partial \rho U_j}{\partial x_i} \right) \right] = -\frac{\partial p''}{\partial x_i} - \frac{\partial}{\partial x_j} (\rho \underline{u_i u_j}) + S_{M_i} \quad (19)$$

where

$$p'' = p + \frac{2}{3} \mu \frac{\partial k}{\partial x_k} \quad (20)$$

The transport equations of RSM can be written as [31]:

$$\begin{aligned} \frac{\partial \rho \underline{U_i U_j}}{\partial t} + \frac{\partial k}{\partial x_k} (\underline{U_k \rho U_i U_j}) = \frac{\partial}{\partial x_k} \left[\left(\rho \underline{U'_i U'_j U'_k} + \rho' (\delta_{kj} U'_i + \delta_{ki} U'_j) \right) \right] + \frac{\partial}{\partial x_k} \left[\mu \frac{\partial}{\partial x_k} (\underline{U'_i U'_j}) \right] \\ - \rho \left(\underline{U'_i U'_k} \frac{\partial u_j}{\partial x_k} + \underline{U'_j U'_k} \frac{\partial u_i}{\partial x_k} \right) - \rho \beta (g_i \underline{U'_j \theta} + g_j \underline{U'_i \theta}) \\ + P' \left(\frac{\partial u'_i}{\partial x_j} + \frac{\partial u'_j}{\partial x_i} \right) - 2\mu \frac{\partial u'_i}{\partial x_k} \frac{\partial u'_j}{\partial x_k} - 2\rho \Omega_k (\underline{U'_j U'_m} \varepsilon_{ikm} + \underline{U'_i U'_m} \varepsilon_{jkm}) \\ + S_{user} \end{aligned} \quad (21)$$

2.3 Wind Inflow Condition

For the three validations and campus studies, the velocity inlet was set up by the power law:

$$\frac{U}{U_0} = \left(\frac{Z}{Z_0} \right)^\alpha,$$

where U is the wind velocity at the height of Z and U_0 is the reference wind speed simulated at the reference height Z_0 without the presence of the building; Z is the vertical distance from the ground. Pressure outlet was used as the outflow condition, the ground was set as the non-slip wall boundary condition, and symmetries were set up for the sides and top boundaries.

Various turbulence models were applied in the first two validation cases. Detailed information was given in the previous section for the governing equations as well as the comparison for the turbulence models adopted in this study.

3. MODEL VALIDATION WITH WIND TUNNEL EXPERIMENT

3.1 One Building Case

3.1.1 Geometry and Mesh for One Building

The three-dimensional CFD model was first developed to simulate urban wind flow around a single building test case. The buildings were configured to follow the wind tunnel tests conducted by Wiren et al. [14].

For the case concerning wind flow around a single building, the detailed building configuration is illustrated in Figure 1a. The building had a length (L) of 80m, a height (H) of 18m, and a width (B) of 12m. At the pedestrian level, there is a pedestrian crossing with a length (B) of 12m, a width (b) of 6m, and a height (h) of 4m in the center of the building.

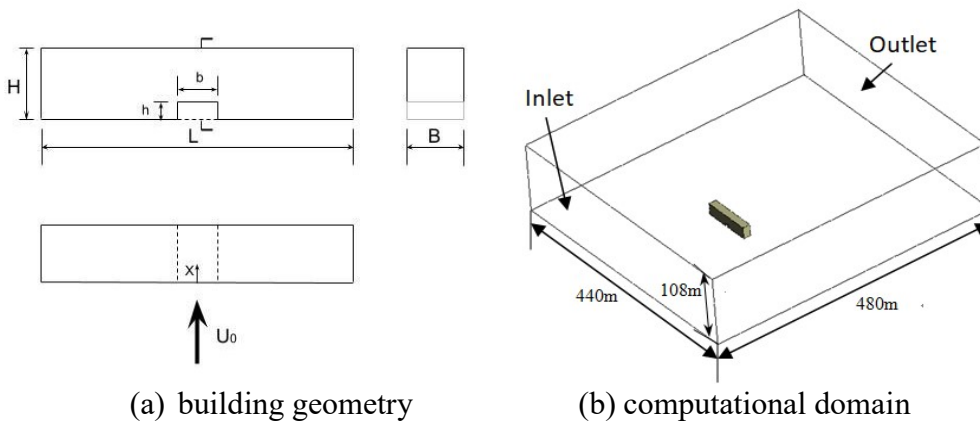


Figure 1. Configuration for single building wind flow validation case

These wind tunnel experiments were measured at the height of 2m at the middle line of the pedestrian channel. Figure 1b shows the computational domain size is 480 m × 440 m × 108 m. To avoid boundary influences, the distance from the inlet to the front surface and all of the side surfaces of the building to the boundaries of the computational domain was 10H. To make sure the flow reached a fully developed condition, the distance from the back surface of the building to the outlet was 16H.

3.1.2 Boundary Conditions

To compare the performance of different turbulence models when simulating urban wind flow, different turbulence models were adopted for urban wind flow simulations in this single-building case. The tested turbulence models were the RNG k- ϵ model, realizable k- ϵ model, k- ω SST model, and second-order Reynolds Stress model. The simulation results were compared with experimental results from wind tunnel tests by Wiren et al. [14].

Boundary conditions applied in single building case wind flow simulation were listed in table 1.

Table 1. Boundary conditions

Zone	Boundary Type	Profile
Inlet	Velocity-inlet	User-defined function
Outlet	Pressure-outlet	Backflow Turbulent Intensity (%): 5 Backflow Turbulent Viscosity Ratio: 10
Top	Symmetry	N/A
Bottom	No-slip wall	Roughness height: 0 Roughness constant: 0.5
Sides	Symmetry	N/A
Building surface	No-slip wall	Roughness height: 0 Roughness constant: 0.5

For the this validation case, the inlet velocity was set up using the power law $\frac{U}{U_0} = \left(\frac{Z}{Z_0}\right)^\alpha$. Based on Wiren's wind tunnel experiments [14], U_0 (10m/s) was the reference velocity and Z_0 (2m) was the reference height, respectively; α was 0.125, and U is the velocity at vertical distance Z from the ground surface. The pressure outlet was used as the outflow condition, the ground was set as a non-slip wall condition, and symmetry was set up for all the sides and top boundaries.

3.1.3 Comparison of Simulation Results for Various Turbulence Models with Wind Tunnel Testing Data

Figure 2a shows the meshes of the computational domain and Figure 2b shows the zoomed-in view of the meshes along the building. The boundary layer meshes that were generated are noticeable, along with the fine meshes around the building for enhanced capturing of the

boundary layer flow features. Three influence regions were selected: around the pedestrian passage with a mesh size of 0.5m, around the building with a mesh size of 1m and another near the upstream and downstream region with a mesh size of 2m. The rest of the computational domain mesh size was 10m in total, 10 inflation layers were used with a 1.2 growth rate. A mesh-independent study was conducted. The medium-sized mesh was adopted in the simulation for different turbulence models as it brought a good balance between the computational accuracy and cost. The total number of elements used in the ultimate simulation for the medium mesh was 2,189,837.

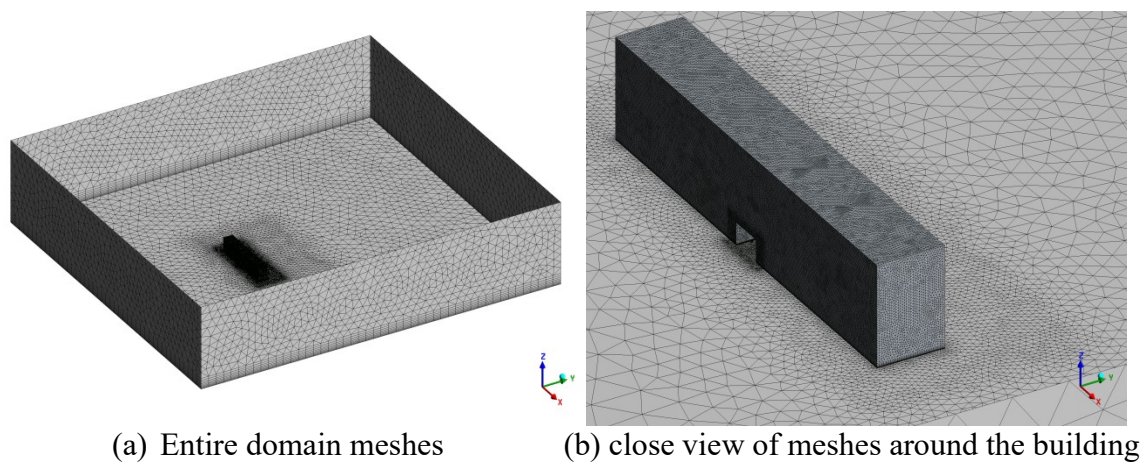


Figure 2. Computational mesh for single building case

An incompressible transient simulation was conducted. The time-averaged velocity contour at a height of 2m from the ground is shown in Figure 3. The pedestrian crossing wind speed was higher than its nearby regions due to the reductions in the cross-sectional area because of a passage at the pedestrian level.

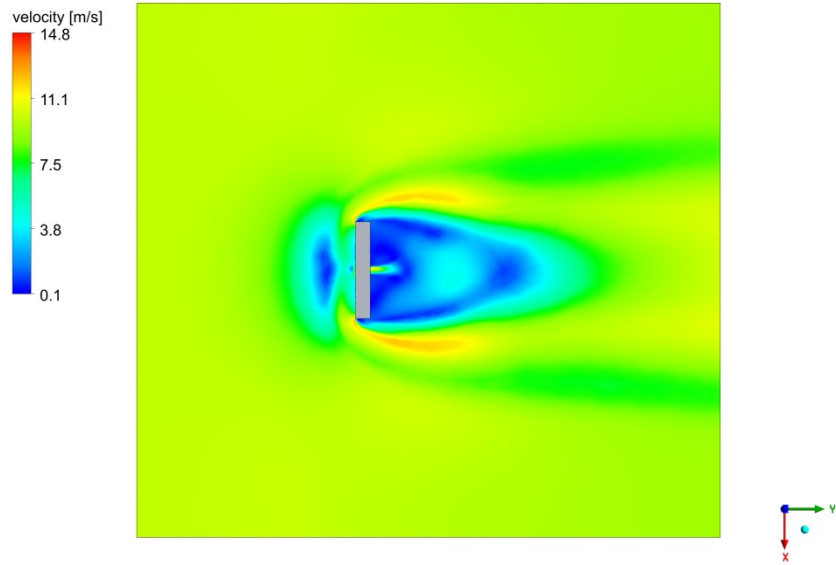


Figure 3. Flow field around the building

Figure 4 and Table 2 show the comparison between the simulation results from different turbulence models and the experimental data. For the single building validation case, the simulation results from all the tested turbulence models showed overall similar trends to the experimental data. The realizable $k-\epsilon$ model and the second-order RSM model showcased better matches. The position of the maximum wind speed was also accurately captured compared with the wind tunnel testing results.

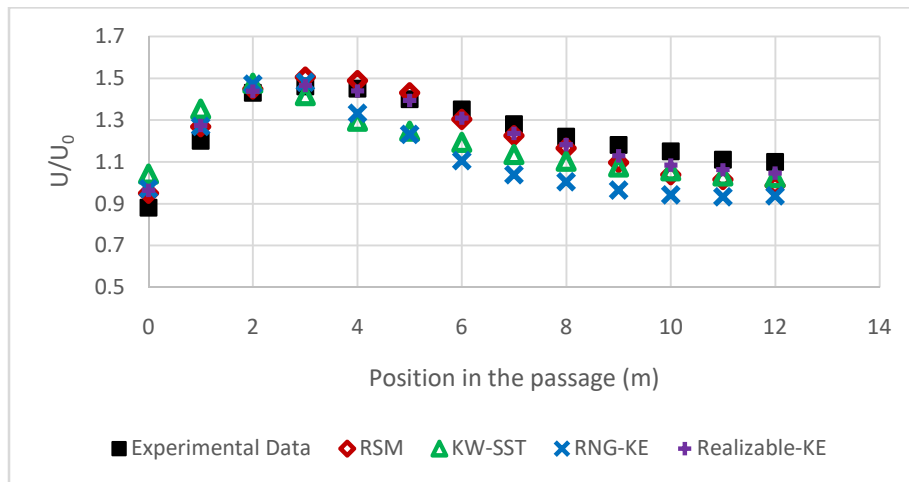


Figure 4. Comparison of simulation results for various turbulence models and wind tunnel testing data.

Table 2. The comparison between different turbulent models for single building case

Turbulence Model	Max Relative Error
Realizable k-epsilon	9.42%
$k-\omega$ SST	18.37%
RNG k-epsilon	18.86%
RSM	10.28%

3.2 Two Buildings Case

3.2.1 Geometry and Mesh for Two Buildings Case

For the case concerning wind flow around two buildings, the building layout is shown in Figure 5. Two identical buildings were arranged perpendicular to each other. The buildings were separated by a passage with distance b is 4m. The wind was blowing perpendicular to the front line formed by the two buildings.

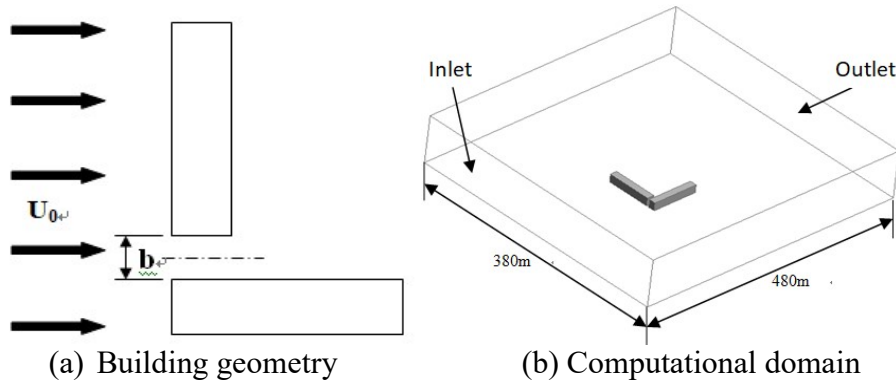


Figure 5. Configuration for two buildings wind flow validation case

Similarly to the previous case, a sufficiently large computational domain was set up, with a height of 108m, a length of 480m, and a width of 380m. The distance from the inlet to the front surface of the building and the building side surfaces to the boundaries of the computational domain was 10H. For this validation study, the downstream of the building was 16H.

3.2.2 Boundary Conditions

Boundary conditions applied in two building case wind flow simulation were similar to single building case.

The tested turbulence models were also the RNG $k-\epsilon$ model, realizable $k-\epsilon$ model, $k-\omega$ SST model, and RSM model. Simulation results were compared with experimental data from wind tunnel tests by Wiren et al. [14].

3.2.3 Comparison of Simulation Results for Various Turbulence Models with Wind Tunnel Testing Data

Similarly, the wind flow for the two-building case was simulated by using the RNG $k-\epsilon$ model, realizable $k-\epsilon$ model, $k-\omega$ SST model, and second-order RSM. The computational meshes for the entire domain is shown in Figure 6a and a close-up view of the refined meshes around the two buildings and the passage is shown in Figure 6b. A similar meshing strategy was used as in the single building validation case. The total element number for the intermediate mesh was 2,242,748.

Velocity contour at the height of 2m from the ground is present in Figure 7. The stagnation region in front of the building, acceleration regions on the windward sides of the building, the passage, and the wake region behind the buildings can all be observed clearly.

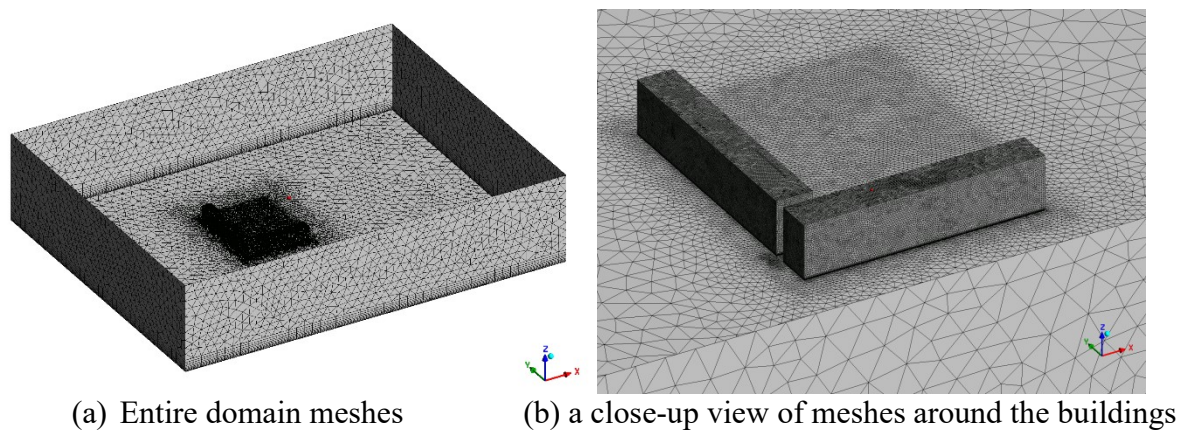


Figure 6. Computational mesh for two buildings case

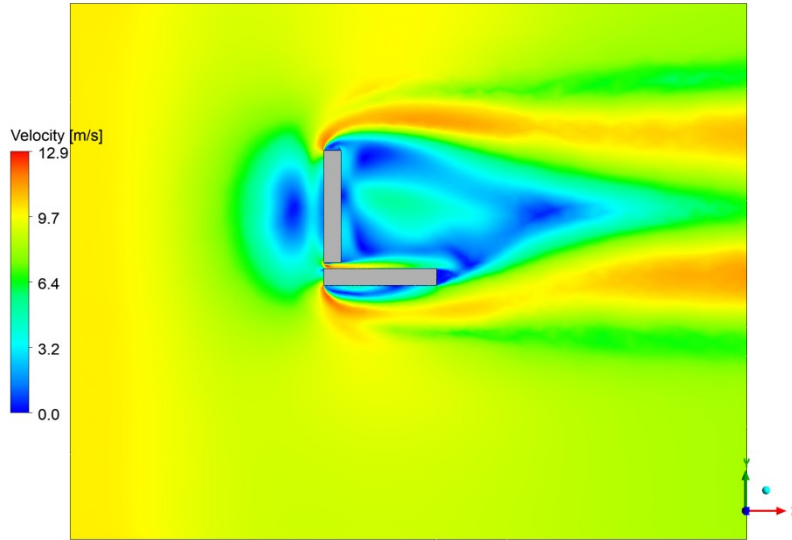


Figure 7. Flow field around the building

The simulation results of the wind speed at 2m high along the central line of the passageway between the two buildings were compared with experimental data [14], as shown in Figure 8 and Table 3. Except for the results obtained by using the second-order RSM, the results of realizable k-epsilon, RNG k-epsilon, and k-omega SST turbulence models did not show good agreement with the experimental data.

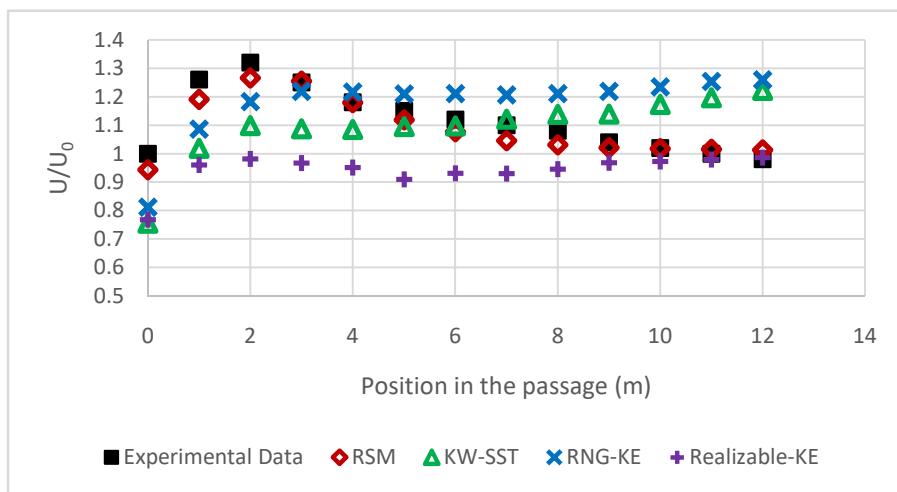


Figure 8. Comparison of simulation results for various turbulence models and wind tunnel testing data

Table 3. The comparison between different turbulent models for two buildings case

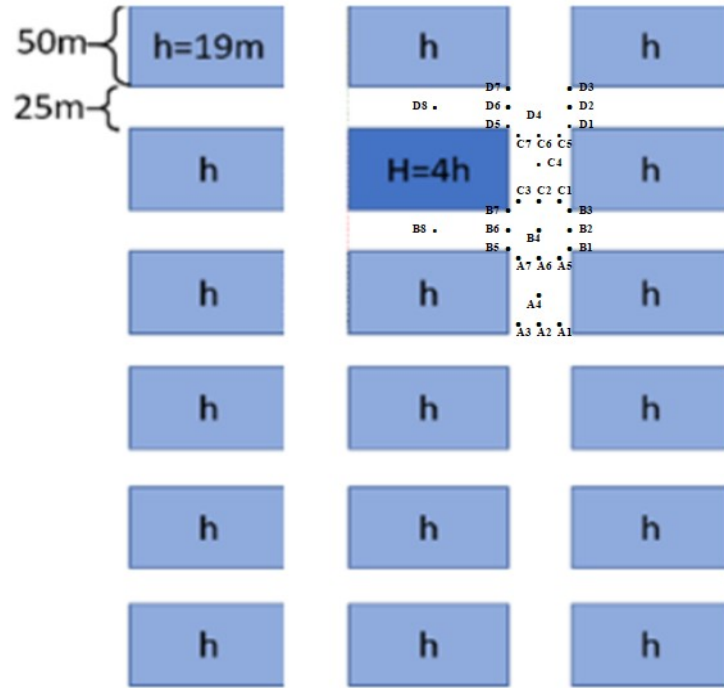
Turbulence Model	Max Relative Error
Realizable k-epsilon	25.62%
k-omega SST	24.65%
RNG k-epsilon	28.53%
RSM	5.6%

From this benchmark case, the RSM continuously showed good computational results for wind flow in this environment and was therefore adopted in the following dense urban wind flow simulation.

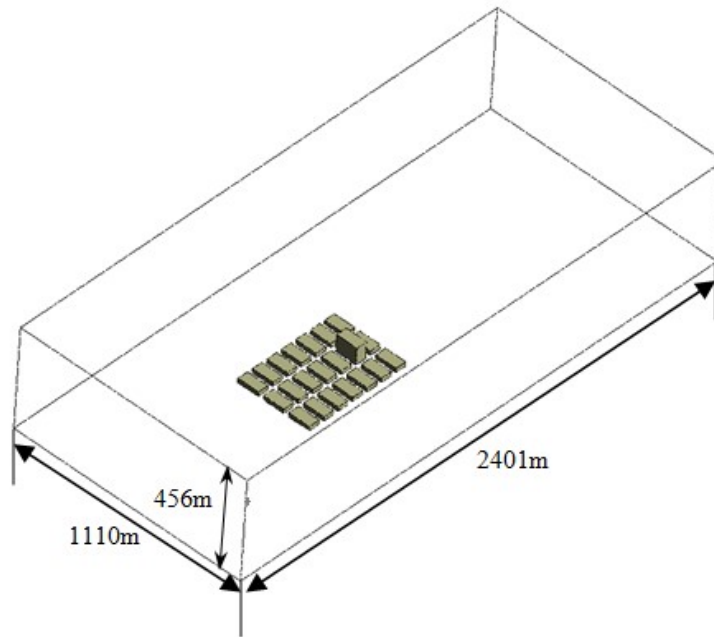
3.3 Wind in A Dense Urban

3.3.1 Geometry and Mesh for A Dense Urban

The figure 9a below shows the configuration for a dense urban and the position of the area measured (A1~D8 points) in the wind tunnel tests [33]. In this simulation, buildings were modeled in two different heights: most are set to 19 meters high (h) and one of them is 76 meters high (H), which is four time of surrounding buildings. Five points groups, A1 to A7, B1 to B8, C1 to C7, and D1 to D8, are measurement points for comparison with the result of wind tunnel tests. Streets have a width of 25 meters. Buildings have a length of 100 meters and a width of 50 meters. The computational domain is shown in Figure 9b.



(a) Configuration for dense urban



(b) Computational domain

Figure 9. Configuration for a dense urban wind flow validation case

Similarly, a sufficiently large calculation domain was created, with a height of 456m, a length of 2401 m, and a width of 1110m. The distance from the inlet to the front surface of the building is 10H, the distance from the building side surfaces to the boundaries of the computational field is 5H for this validation simulation, and the downstream of the building is 16H.

The size of the domain should be set to prevent diverse effect of the surrounding boundaries, such as reserved flow. The domain size namely the length of 10H upstream of the building, the length of 15H downstream and the length of 6H height.

In terms of mesh size and number of grids, the medium mesh is recommended in this case, which brought a good balance between the cost and simulation accuracy. The total number of mesh cells is approximately 17.12 million.

3.3.2 Boundary Conditions

The inlet boundary condition is listed as below:

$$\frac{U}{U_0} = \left(\frac{z}{z_0}\right)^\alpha ;$$

where $Z_0=2m$, $U_0=10m/s$ and $\alpha=0.25$.

The outlet was set up as pressure outlet and the calculation method was chosen SIMPLE second order upwind method. In addition to the velocity profile, the turbulence parameters at the inlet also should be defined. RSM model was chosen for this case. Boundary conditions applied in a dense urban case wind flow simulation were listed in table 4.

Table 4. Boundary conditions

Zone	Boundary Type	Profile
Inlet	Velocity-inlet	User-defined function
Outlet	Pressure-outlet	Backflow Turbulent Intensity (%): 5 Backflow Turbulent Viscosity Ratio: 10
Top	Symmetry	N/A
Bottom	No-slip wall	Roughness height: 0 Roughness constant: 0.5
Sides	symmetry	N/A
Building surface	No-slip wall	Roughness height: 0 Roughness constant: 0.5

3.3.3 Comparison of Simulation Results for Various Turbulence Models with Wind Tunnel Testing Data

Similar to the above cases, wind flow in a dense urban case was simulated by using a 2nd order RSM. The computational mesh for the entire domain is shown in Figure 10a and a close-up view of the refined mesh around the buildings and the passages is shown in Figure 10b. Similar meshing strategies were used as the single and two building validation cases. The total element number for the medium mesh is 17,126,549. The time-averaged velocity contour at a height of 2m from the ground is shown in Fig. 11. The pedestrian crossing wind flow can be observed clearly in Figure 11b.

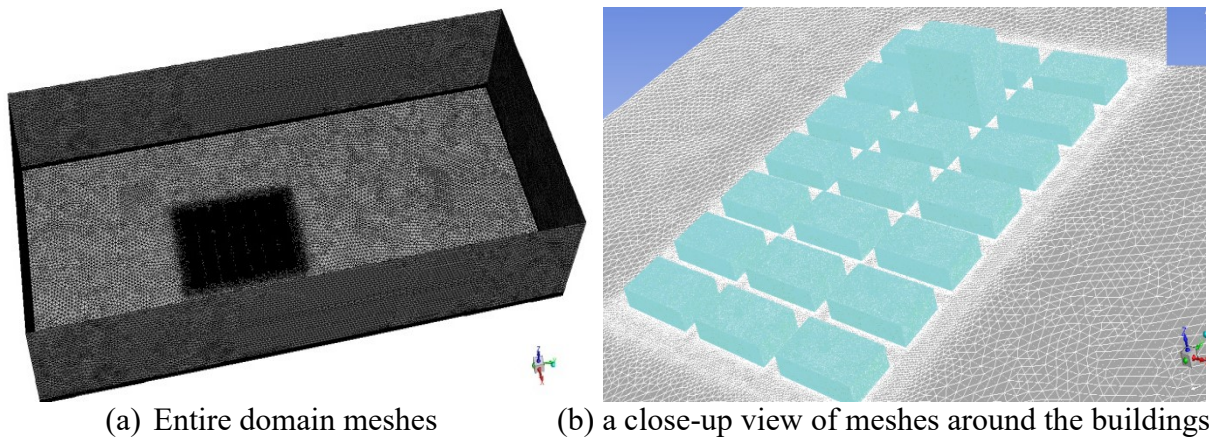
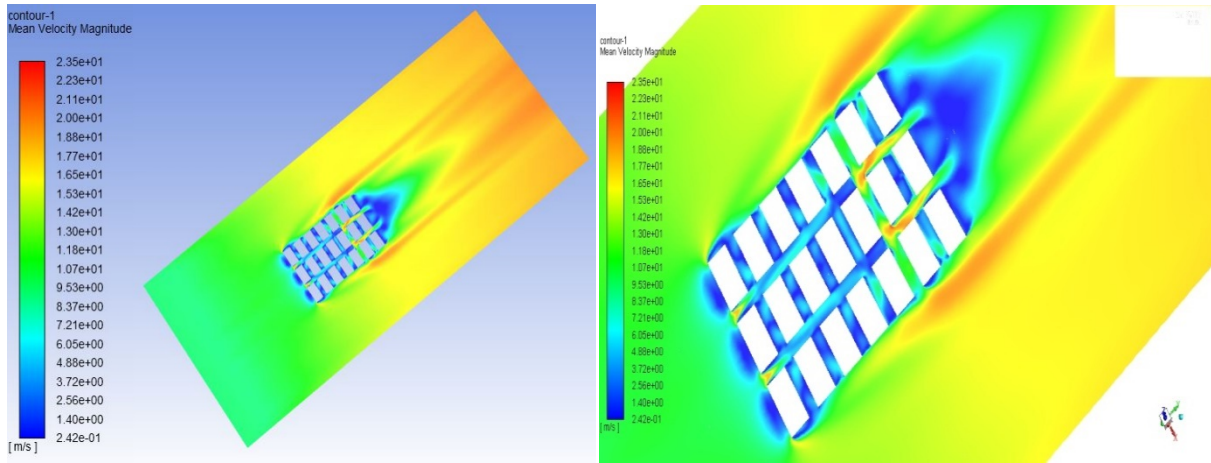


Figure 10. Computational mesh for dense urban case



(a) Flow field around the building; (b) a close-up view of flow field around the buildings

Figure 11. Flow field around the building

Simulation results of velocity at 2m high in the passage were compared with wind tunnel test data [33] as shown in Fig. 12 and Table 5.

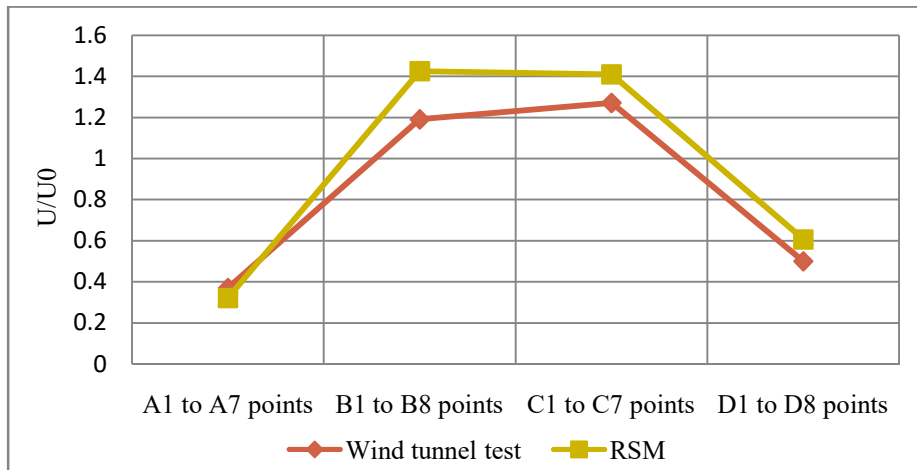


Figure 12. Comparison of simulation results for RSM turbulence model and wind tunnel testing data

Table 5. The comparison between different turbulent models for building density case

Simulation area	Relative Error
Mean U/U_0 for A1 to A7 points	13.08%
Mean U/U_0 for B1 to B8 points	19.75%
Mean U/U_0 for C1 to C7 points	10.98%
Mean U/U_0 for D1 to D8 points	21.33%

From the three benchmark cases, the RSM showed better simulation results for wind flow in the urban environment and was also adopted in the following urban wind flow simulation and wind turbine siting study.

Realizable and RNG $k-\epsilon$ model shows better performance than the standard $k-\epsilon$ model in strong streamline bending, vortex and rotation. The current research shows that the realizable $k-\epsilon$ model can solve flow separation and complex secondary flow well in all $k-\epsilon$ models.

A huge shortcoming of the realizable $k-\epsilon$ model is that it cannot provide natural turbulent viscosity when calculating rotating and static flow regions, because the realizable $k-\epsilon$ model considers the influence of the average curls when defining the turbulent viscosity. Because of these modifications, it needs attention to apply it to multiple reference systems.

For many complex flows around buildings, such as stagnant areas, strong pressure gradients, separated flows, very curved motions, etc., the RSM method designed to produce better results than its predecessor. [30-31]

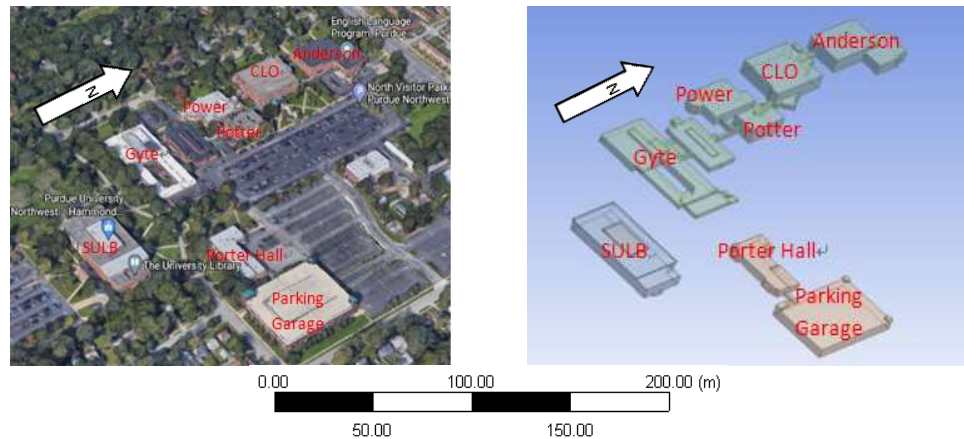
In Fluent, the Reynolds Stress turbulence model is particularly suitable for wind conditions in suburban and urban areas, including uneven building height. Therefore, it provides good results for the passage between buildings and the average wind speed in the entire urban environment, [29]

4. 3-D WIND FIELD CONSTRUCTION

4.1 Geometry of PNW Campus Buildings

Purdue University Northwest (PNW) is located in Northwest Indiana, a suburban environment. An urban wind flow simulation for PNW was conducted to help identify the optimal location of a VAWT on campus.

Figure 13a shows the top view of the campus environment from Google Maps and Figure 13b shows the layout of the campus's main buildings. The main buildings include the Student Union and Library Building (SULB), Gyte building, Porter Hall, Parking Garage building, Power building, Potter building, Classroom Office building (CLO), and Anderson building. All the main buildings were included in the three-dimensional urban wind field geometry models. To reduce the complexity of meshing and further computational efforts, some detailed building structures were neglected.



(a) Top view from Google Maps

(b) The building layout 3-D model.

Figure 13. Overview of the Purdue University Northwest (PNW) campus buildings

The computational domain was 740 m in length, 630 m in width, and 100 m in height. It was selected to avoid the boundary effects around the inflow and sides, and to make sure the downstream reached a fully developed flow region. The distance from the inlet to the SULB

front surface was $8H$, $16H$ downstream, $5H$ on each building side, and about $5H$ above the building's roof. The tallest building height (H) was 17.27m .

To monitor the on-campus wind flow conditions, three wind sensors were installed on the roof of the SULB. The height of the SULB was 16.43m , the location of each data sensor is shown in Figure 14. Figure 15-21 show the details for each building and building layout.

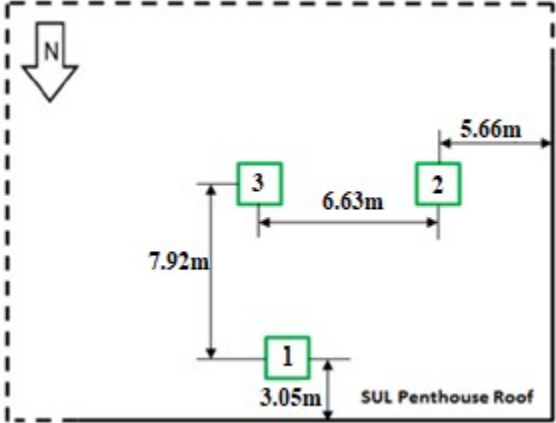


Figure 14. Location of three wind data sensors

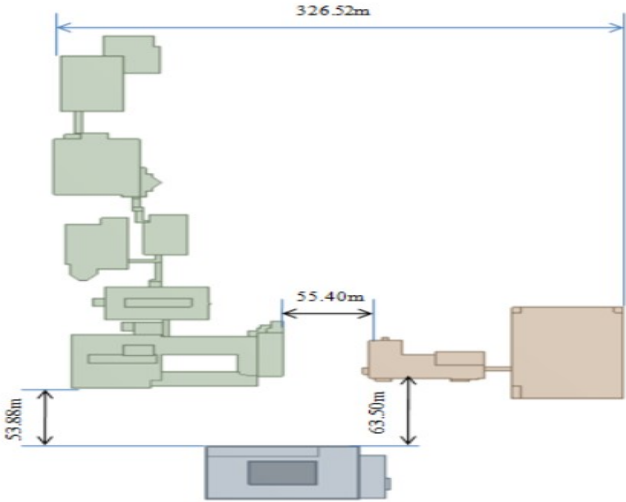
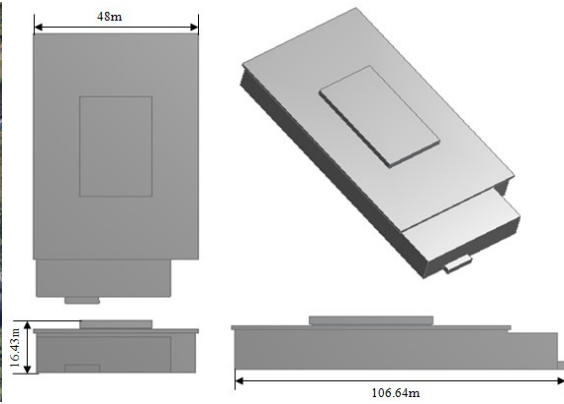


Figure 15. 3-D model at different view of building layout



(a) View from Google Map

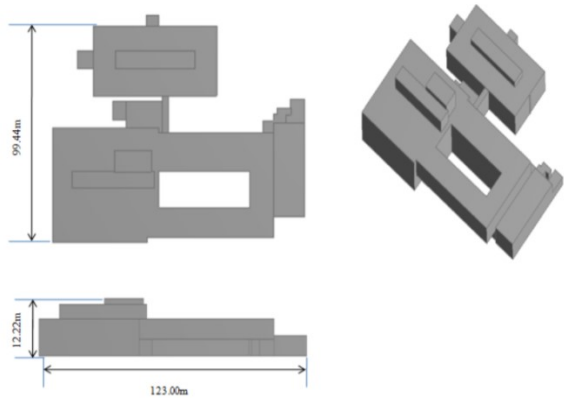


(b) 3-D SULB model at different view

Figure 16. Overhead view of SULB



(a) View from Google Map

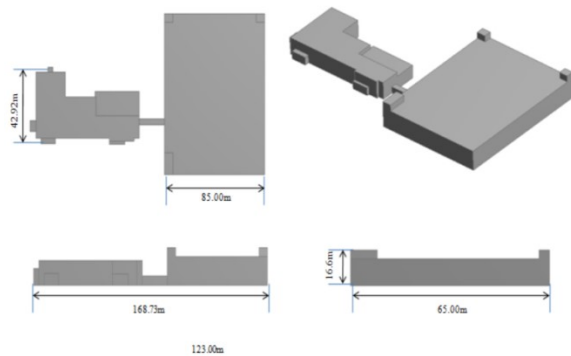


(b) 3-D Gyte building model at different view

Figure 17. 3-D Gyte building model at different view



(a) View from Google Map

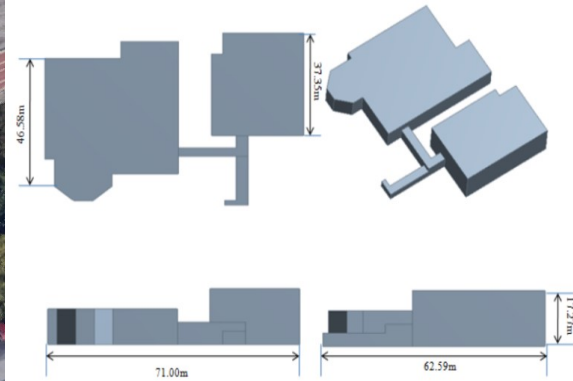


(b) 3-D Porter Hall and Parking Garage model at different view

Figure 18. 3-D Porter Hall and Parking Garage model at different view



(a) View from Google Map

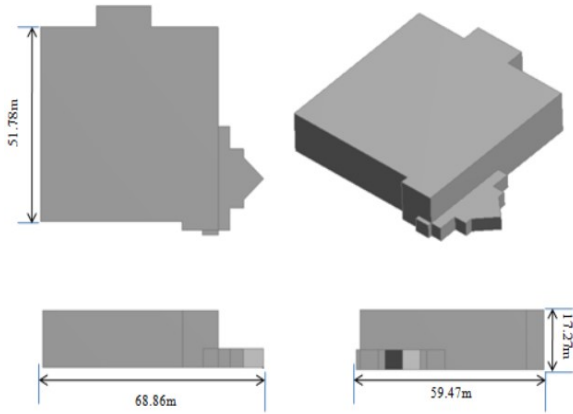


(b) 3-D Potter and Power building model at different view

Figure 19. 3-D Potter and Power building model at different view



(a) View from Google Map

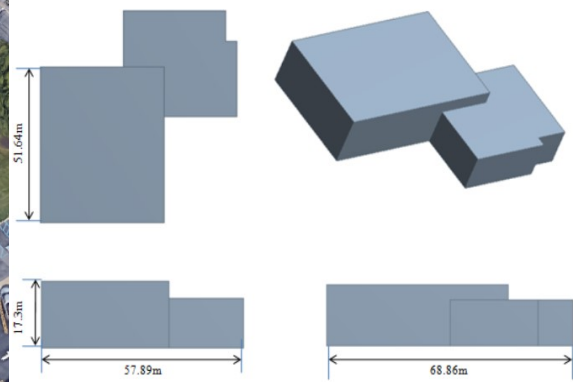


(b) 3-D CLO building model at different view

Figure 20. 3-D CLO building model at different view



(a) View from Google Map



(b) 3-D Anderson building model at different view

Figure 21. 3-D Anderson building model at different view

4.2 Mesh Generation

Three different sets of mesh were used for the mesh-independent study, where the element numbers were 2,673,927, 7,826,295, and 12,095,887 for coarse (surface element size 0.8m, body element size 5m), medium (surface element size 0.5m, body element size 5m), and fine mesh (surface element size 0.4m, body element size 3m), respectively. The simulation results obtained from the medium mesh and fine mesh did not show much difference. The medium mesh was adopted in the simulation as it brought a good balance between computational accuracy and cost.

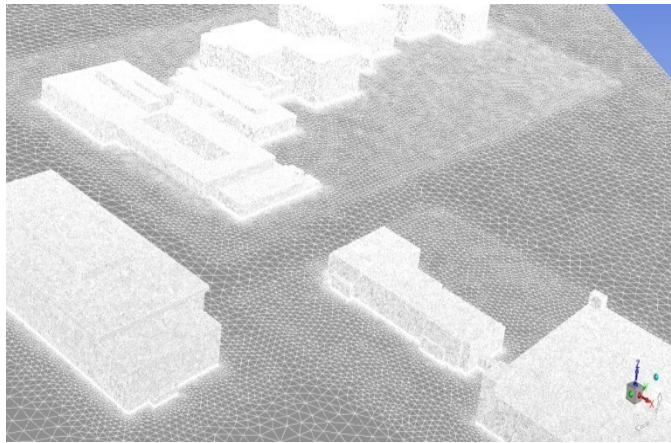


Figure 22. Mesh detail: mesh detail of SULB and surrounding buildings

4.3 Boundary Conditions

The boundary conditions applied in the PNW campus wind flow simulation were listed in Table6.

Table 6. Boundary conditions

Zone	Boundary Type	Profile
Inlet	Velocity-inlet	User-defined function
Outlet	Pressure-outlet	Backflow Turbulent Intensity (%): 5 Backflow Turbulent Viscosity Ratio: 10
Top	Symmetry	N/A
bottom	No-slip wall	Roughness height: 0 Roughness constant: 0.5
Sides	Pressure-outlet	Backflow Turbulent Intensity (%): 5 Backflow Turbulent Viscosity Ratio: 10
Building surface	No-slip wall	Roughness height: 0 Roughness constant: 0.5

The prevailing wind speed and wind direction were determined based on an analysis of year-long wind data [1] from the three data sensors. Recorded wind data from April 2010 to April 2011 were used. After the prevailing wind information was determined, the inflow wind profile was setup. As explained before, the inlet velocity profile is defined by using the 1/7 power law as:

$$U = U_0 (z/19)^{1/7}, U_0 = 3.17 \text{ m/s.}$$

The outlet was a pressure outlet and the other two sides of the domain were also regarded as pressure outlets. The ground was the bottom of the computational domain and was therefore treated as a no-slip wall. The building walls were considered to be smooth no-slip wall boundary conditions. The top boundary of the computational domain was set as a symmetry condition.

5. URBAN WIND FLOW ANALYSIS

5.1 3-D Wind Field Simulation Results for Wind Turbine Citing

In order to identify the most ideal siting location for the wind turbine, three-dimensional wind fields for PNW were constructed. Based on the validation results, RSM was selected for the PNW urban wind flow simulation.

Figure 23 shows the velocity contour at a height level of 21m. It represents the average height of the selected turbine (half of the rotor height) on different building's roof.

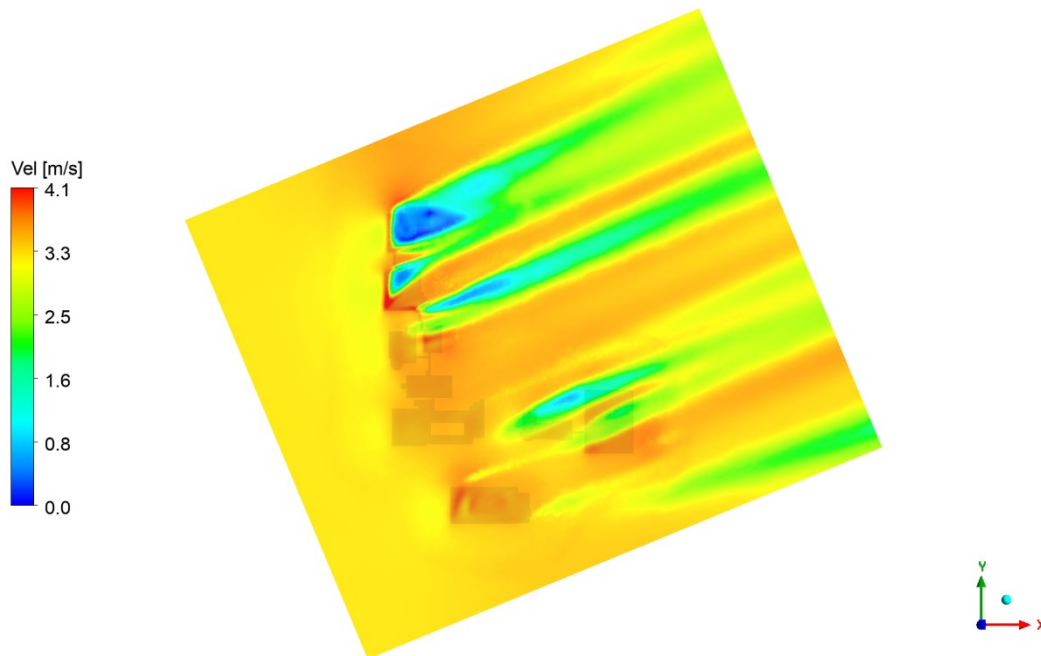


Figure 23. Contour of wind velocity at height level 21m

At a height level of 21m, the SULB showed good wind potential. Even though the CLO and Anderson buildings were higher than the SULB, at the height level of 21m, the wind flow above the CLO and Anderson buildings were at the lower part of the boundary layer flow region, which showed lower wind potential compared to the same height as the SULB. Among all the buildings on PNW's campus, the SULB can be seen as a good candidate for siting the turbine when comparing wind energy potentials.

A side view of the wind flow around the SULB is shown in Figure 24. When the wind blows over the edges of a building, the flow will separate at the leading edge of the roof at a certain angle, referred to as the skew angle. The low was accelerated because of the separation effects. Furthermore, serving as the foundation of the wind turbine, the special penthouse structure on top of the SULB edge can also increase the wind potential due to the skew angle effects; therefore, an optimal location for wind turbine siting was proposed.

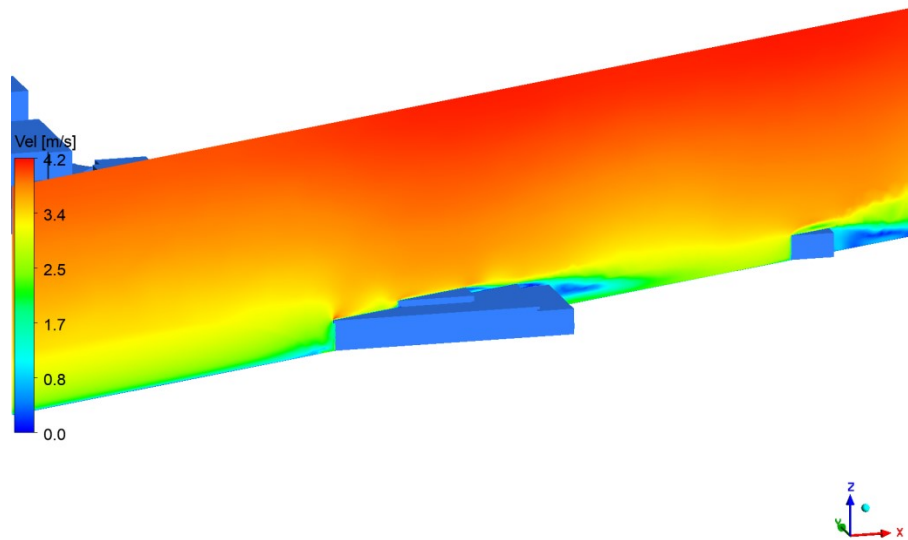
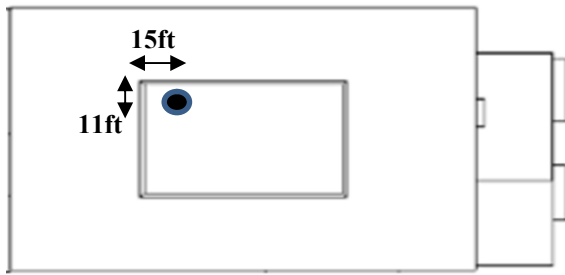


Figure 24. Contour of wind velocity around SUL Building

After considering the simulation results, support capability of the roof structure, existing objects on top of the building roof, available budget, and overall aesthetic look, a small-scale VAWT was installed on the roof of the SULB. Figure 25a shows the final selection of the wind turbine siting location on top of the SULB, while Figure 25b shows a picture of the final installation.



(a) Suggested Installation location



(b) Selected Installation Site



(c) Sensor on the SULB

Figure 25. Wind turbine installation location

The Eddy GT wind turbine from Urban Green Energy (New York, NY, USA location) was available to be installed on the top of the PNW campus buildings' roofs. With the advantages of being lightweight and producing a low amount of noise, this small-scale vertical axis wind turbine (VAWT) has been used for residential and commercial applications in various regions in the United States. The rated power for this wind turbine is 1kW.

The detailed properties and performance information of that wind turbine, as stated by the manufacturer, are given in Table 7. The total height of the turbine was 4.70m.

Table 7. Eddy GT wind turbine properties and specifications

Axis	Vertical
Height	2.70 m
Tower height	2 m
No. of blades	3
Width	1.80 m
Weight	175 kg
Swept Area	4.62 m ²
Cut-in wind speed	3 m/s
Cut-out wind speed	30 m/s
Rated wind speed	12 m/s
Survival wind speed	55 m/s
Rated power	1000 W

The Eddy GT wind turbine power output curve shown in Figure 26 indicates the amount of power that could be extracted from the wind turbine at different wind speeds. The extracted power can be calculated using $PT(V_w) = P_r \frac{V_w^3 - V_1^3}{V_r^3 - V_1^3}$ (V_w is the wind speed, P_r is the wind turbine rated power, V_1 is the cut-in wind speed, and V_r is the rated wind speed) when the wind speed is greater than the cut-in speed and smaller than the rated speed. If the wind speed is greater than or equal to the rated wind speed and less than the cut-out speed, the rated power will be extracted from the wind turbine.

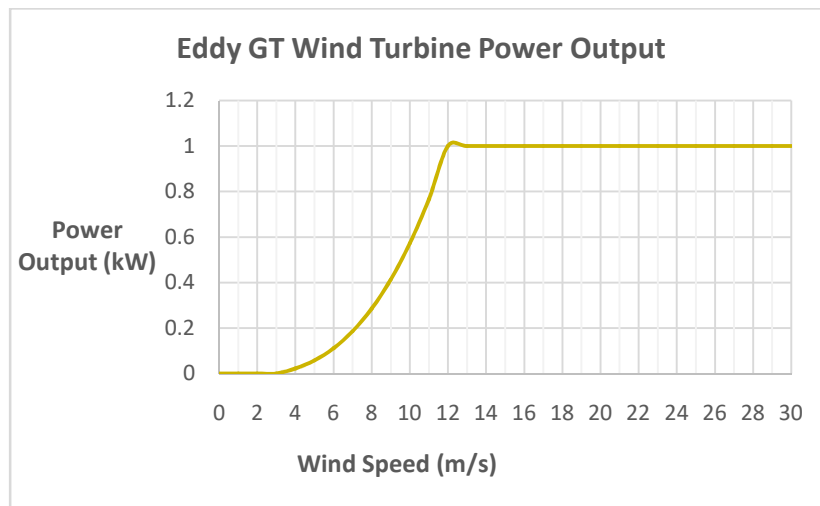


Figure 26. Eddy GT Wind Turbine power output curve.

Based on the power output curve of the wind turbine and the wind velocity probability density on the installation site, the estimated power generation of the wind turbine can be calculated.

In an ideal situation, the wind turbine should be installed in a site where the rated wind speed has a high probability. Based on the wind data analysis, the wind energy potential on the PNW campus was not very high, as the annual (from April 2010 to April 2011) averaged wind speed was 2.67 m/s, which is lower than the cut-in wind speed. The Eddy GT Wind Turbine, which is on SUL Building will not fully perform under this given wind condition. Over the year (April 2010 to April 2011), there were seven months that had an average wind speed higher than the cut-in wind speed. Wind power was expected to be generated during these periods. Due to some constraints, the wind turbine was selected even though it did not meet all the desires. In conclusion, the selection of a wind turbine is a complex decision and should be made with consideration of the wind potential, availability of resources, and budget constraints.

5.2 The Wind Comfort Analysis at Pedestrian Level

People would feel uncomfortable when the wind speed is greater than 3.5m/s at pedestrian level in town [34]. The wind velocity over from 3.5m/s can make people hair disturbed, clothing flaps.

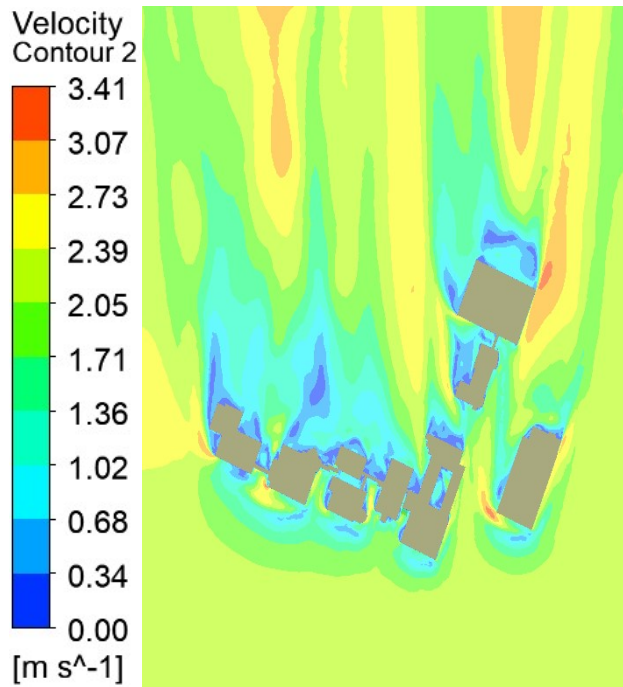


Figure 27. Contour of wind velocity at height of 2m from ground

The contours in Figure 27 illustrated that the airflow climbed over the buildings and caused turbulent flow and vortex in front of and behind the building.

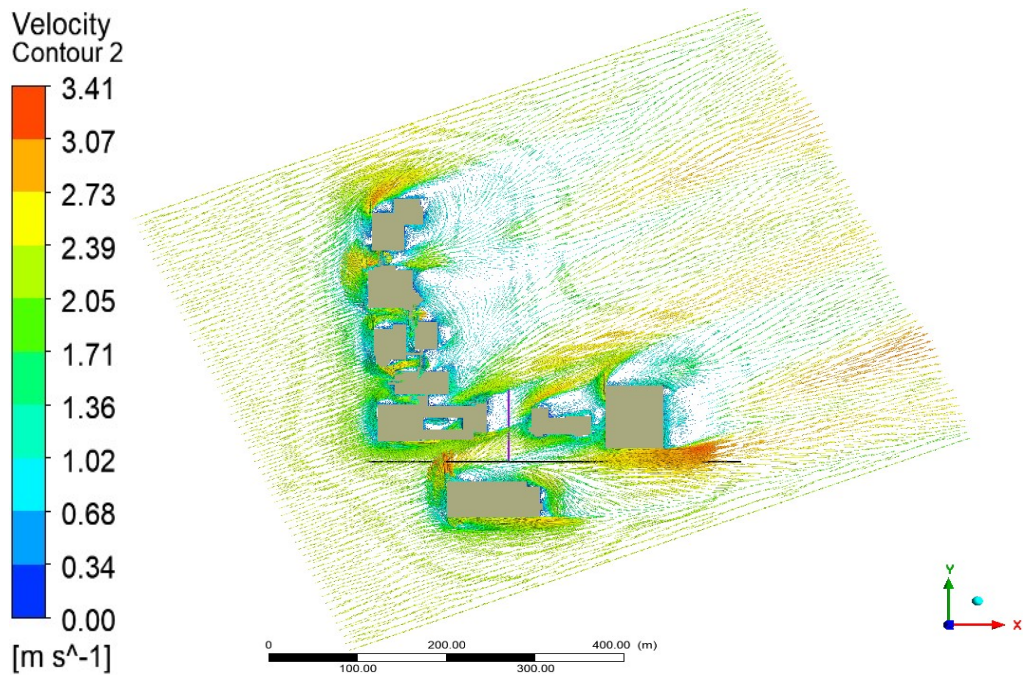
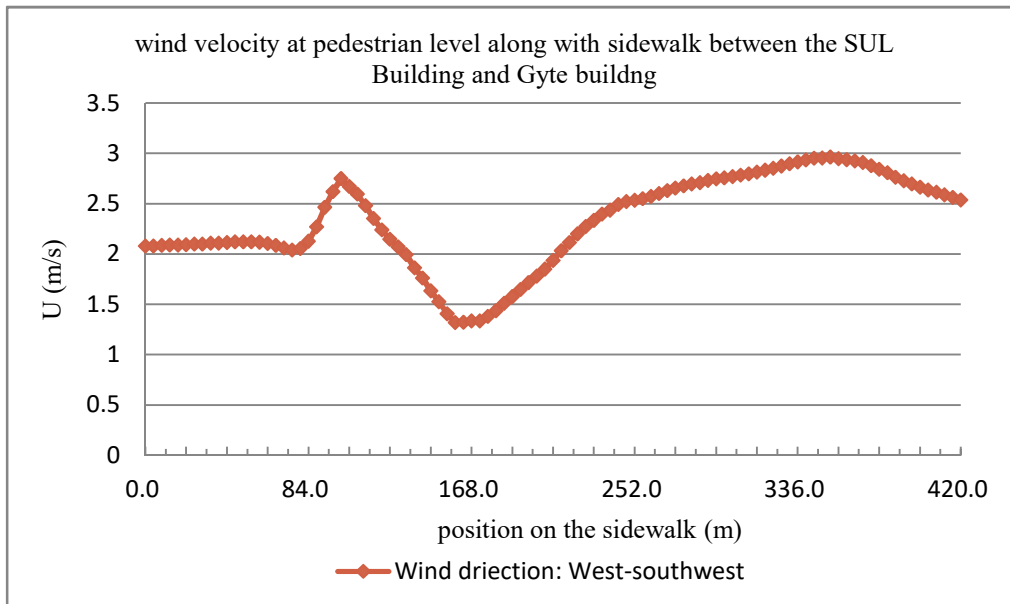


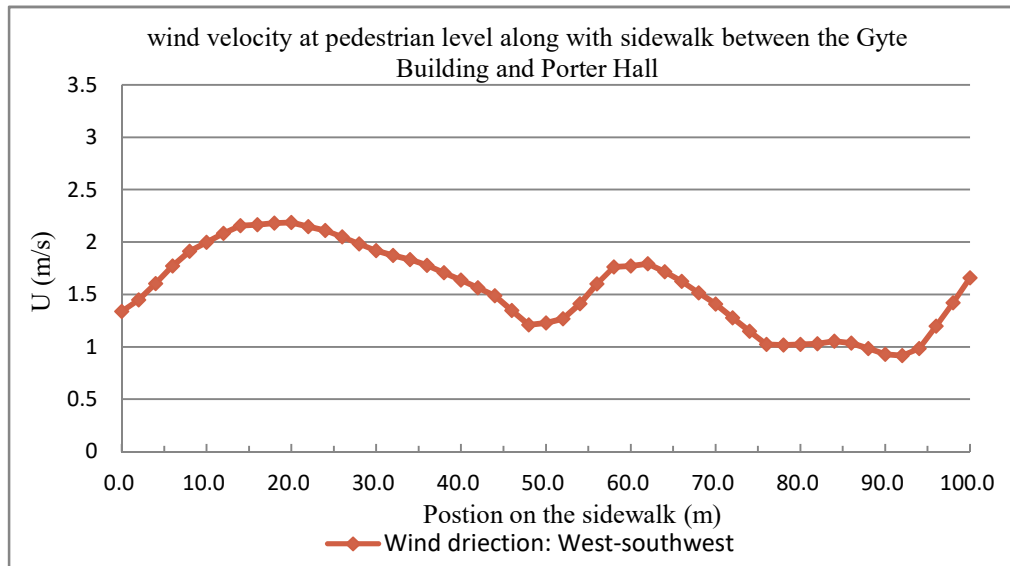
Figure 28. Wind velocity vector at height of 2m from ground

Figure 28 shows wind velocity vectors at pedestrian level. The black line is the central line which is the sidewalk (420m) between the SUL building and Gyte Building. It consists of 100 simulation points. The vertical line in Figure 28 is the sidewalk (100m) between Gyte building and Porter Hall; and it contains 50 simulation points. When the wind direction is on West-southwest, the average wind speed along with the path between the SUL building and Gyte building was higher than the average wind speed along with the sidewalk between Gyte building and Porter Hall.

For the purpose of a clear comparison of the effects from wind speed, the wind velocity along with sidewalks is displayed in Figure 29 below.



(a) Between the SUL Building and Gyte building



(b) Between the Gyte building and Porter Hall

Figure 29. Wind velocity at pedestrian level along with sidewalk

The position on the sidewalk between the SUL Building and Gyte building is from the left to right path. For the position on the sidewalk between the Gyte building and Porter Hall is along with y axis in Figure 28. Figure 29 presents the wind speeds on two sidewalks are not exceeding 3.5m/s, so it will not cause people to feel uncomfortable in general.

In the current simulation, only the annual average wind speed is used as setting the inlet boundary condition. Considering the monthly wind speed varies, there are several months with average wind speed bigger than the annual wind speed. As a result, they may lead to uncomfortable level increases even in the same sidewalks studied here.

6. CONCLUSIONS AND FUTURE WORK

A three-dimensional CFD model was developed to simulate wind flow in urban environments. Different turbulence models were adopted to simulate urban wind flow. The simulation results were compared with wind tunnel testing data. The results showed that among all the models tested (RSM, $k-\omega$ SST, realizable $k-\epsilon$, and RNG $k-\epsilon$ models), RSM gave the best matches with experimental data in three benchmark cases. Therefore, RSM was selected to simulate the urban wind flow and wind turbine siting for Purdue University Northwest, which is located in an urban area in Northwestern Indiana.

A one-year wind data analysis result was used to set up the inlet wind profile. The simulation results were used as the wind turbine energy production estimation for the selected wind turbine.

3-D suburban wind characters were studied and analyzed based on wind fields around the SULB. Flow over a building was separated from the roof windward leading edge at a certain skew angle. Wind flow became accelerated due to the flow separation, which may enhance the wind energy potential in that area. Besides serving as the foundation of rooftop wind turbines, buildings may also play an active role in helping to gain more wind energy output in an urban environment.

Furthermore, when considering the wind turbine siting on top of the building roof, a taller building has the benefit of reaching a higher wind power density. However, in order to take advantage of this feature, the selected turbine needs to reach a certain height. Otherwise, due to the lower part of the boundary layer flow effects, a relatively low building may be a better choice for a low-height wind turbine siting.

Small-scale wind turbines are usually lightweight, have low vibrations, and reduced noise. They are widely used in urban environments. Many factors need to be considered for urban wind turbine siting, such as the selected site wind potential, the probability of the wind speed compared to the cut-in wind speed and rated wind speed, the height of the wind turbine vs. the height of the buildings, the building roof structure, and existing objects. The final decision should fit within the budget limits.

In the future work, the influence of local climate on wind characteristics, such as thermal effects, temperature and humidity, can also be considered, that may further improve the simulation accuracy.

REFERENCES

- [1].Lu, L. 3-D Wind Fields Construction for Suburban Environment. Master's Thesis. Purdue University, Hammond, Indiana, August 2012.
- [2].Renewable 2020 Global Status Report, pp.15, Retrieved from, https://www.ren21.net/wpcontent/uploads/2019/05/gsr_2020_full_report_en.pdf
- [3].Manwell, J.F.; McGowan, J.G.; Rogers, A.L. Wind Energy Explained: Theory, Design and Application, 2nd ed.; John Wiley & Sons: Hoboken, NJ, USA, 2002; pp. 55–59.
- [4].Sawin, J.L., 2012, Renewables 2012 Global Status Report, <http://www.map.ren21.net/GSR/GSR2012.pdf>
- [5].Aguilo, A., Taylor, D., Quinn, A. and Wiltshire, R., 2004, Computational Fluid Dynamic Modeling of Wind Speed Enhancement through A Building-augmented Wind Concentration System, European Wind Energy Conference.
- [6].Avila, M., Folch, A., Houzeaux, G., Eguzkitza, B., Prieto, L., Cabezon, D., 2013, A parallel CFD model for wind farms, ICCS 2158-2160.
- [7].Stathopoulos, T., Baskaran, A., 1996. Computer simulation of wind environmental conditions around buildings .Eng. Struct. 18 (11), 876–885.
- [8].Westbury, P.S., Miles, S.D., Stathopoulos, T., 2002. CFD application on the evaluation of pedestrian-level winds. In: Workshop on Impact of Wind and Storm on City Life and Built Environment, Cost Action C14, CSTB, June 3–4, Nantes, France.
- [9].Roache, P.J., K. Ghia, and F. White, "Editorial Policy Statement on the Control of Numerical Accuracy," ASME Journal of Fluids Engineering, Vol. 108, No. 1, March 1986, 2.
- [10]. AIAA, "Guide for the Verification and Validation of Computational Fluid Dynamics Simulations," AIAA G-077-1998, 1998.
- [11]. ERCOFTAC, Best Practices Guidelines for Industrial Computational Fluid Dynamics, Version 1.0, January 2000.
- [12]. Murakami, S., Overview of turbulence models applied in CWE-1997, Journal of Wind Engineering and Industrial Aerodynamics 74-73,1998,1-24
- [13]. Stathopoulos, T.; Alrawashdeh, H.; Al-Quraan, A.; Blocken, B.; Dilimulati, A.; Paraschivoiue, M.; Pilay, P. Urban wind energy: Some views on potential and challenges. J. Wind Eng. Ind. Aerod.2018, 178, 146–157.

- [14]. Wiren, B.G. A wind tunnel study of wind velocities in passages between and through buildings. In Proceedings of the 4th International Conference on Wind Effects on Buildings and Structures, London, UK, September 1975; pp. 465–475.
- [15]. Tsang, C.W.; Kwok, K.C.S.; Hitchcock, P.A. Wind tunnel study of pedestrian level wind environment around tall buildings: Effects of building dimensions, separation and podium. *Build Environ.*2012, 49(3), 167-181.
- [16]. Weerasuriya, A.U.; Tse, K.; Zhang, X.; Li, S. A. Wind tunnel study of effects of twisted wind flows on the pedestrian-level wind field in an urban environment. *Build Environ.*2018, 128, 225–235.
- [17]. Li, J.; Peng, Y.; Ji, H.; Hu, Y.; Ding, W. A. Wind tunnel study on the correlation between urban space quantification and pedestrian–level ventilation. *Atmosphere.*2019, 10(10), 564.
- [18]. Blocken, B.; Carmeliet, J.; Stathopoulos, T. Pedestrian-level wind conditions around buildings: Review of wind-tunnel and CFD techniques and their accuracy for wind comfort assessment. *Build Environ.* 2016, 100, 50–81.
- [19]. Rodi, W. Comparison of LES and RANS calculations of the flow around bluff bodies, J. *Wind Eng. Ind. Aerod.*1997, 69, 55–75.
- [20]. Johnson, G.T.; Hunter, L.J. Urban wind flows: Wind tunnel and numerical simulations-a preliminary comparison. *Environ Modell Softw.*1998, 13, 279–286.
- [21]. Willis, R. Validation of CFD Predictions of Urban Wind. Master’s degree Thesis. Victoria University of Wellington, Wellington, New Zealand, 2017.
- [22]. Song, C.C.; He, J. Evaluation of pedestrian winds in urban area by numerical approach. *J. Wind Eng. Ind. Aerod.*1999, 81, 295–309.
- [23]. Santiago, J.L.; Martilli, A. CFD simulation of airflow over a regular array of cubes. Part I: Three-dimensional simulation of the flow and validation with wind-tunnel measurements. *Boundary Layer Meteorol.*2007, 122, 609–634.
- [24]. Zheng, C.; Li, Y.; Wu, Y. Pedestrian-level wind environment on outdoor platforms of a thousand-meter-scale mega tall building: Sub-configuration experiment and wind comfort assessment. *Build Environ.*2016, 106, 313–326.
- [25]. Gnatowska, R.; Sosnowski, M.; Uruba, V. CFD modeling and PIV experimental validation of flow fields in urban environments. *E3S Web Conf.*2017, 14, 1034.

- [26]. Akashi, M.; Isaac, L. Prediction of wind environment and thermal comfort at pedestrian level in urban area. *J. Wind Eng. Ind. Aerod.* 2006,96(10), 1498-1527.
- [27]. Hu, K.; Cheng, S.; Qian, Y. CFD simulation analysis of building density on residential wind environment. *J. Eng. Sci. Technol. Rev.*2018,11(1),35- 43.
- [28]. Liu, S.; Pan, W.; Zhang, H.; Cheng, X.; Long, Z.; Chen, Q. CFD simulations of wind distribution in an urban community with a full-scale geometrical model. *Build Environ.* 2017, 117, 11–23.
- [29]. Reiter, S. Validation Process for CFD Simulations of Wind around Buildings. Proceedings of the European Built Environment CAE Conference. Available online: <https://scholar.google.com/scholar?hl=en&q=Reiter+S%3A+%282008%29.+%E2%80%9CValidation+Process+for+CFD+Simulations+of+Wind+Around+Buildings%E2%80%9D.+European+Built+Environment+ACE+Conference>.
- [30]. Fluent Theory Guide: Large Eddy Simulation (LES) Model. Available online: https://ansyshelp.ansys.com/account/secured?returnurl=/Views/Secured/corp/v192/flu_th/flu_th_sec_turb_les.html.
- [31]. Fluent Theory Guide: Turbulence. Available online: https://ansyshelp.ansys.com/account/secured?returnurl=/Views/Secured/corp/v192/flu_th/flu_th_chap_turbulence.html.
- [32]. Menter, F.R. Two-equation eddy-viscosity turbulence models for engineering applications. *AIAA J.*1994, 32(8), 1598–1605.
- [33]. Stathopoulos, Th., Wu, H., General models for pedestrian-level winds in built-up regions, *Journal of Wind Engineering and Industrial Aerodynamics* 54/55 (1995), 515-525.
- [34]. Zhang, X.; Tse, K.; Weerasuriya, A.; Li, S.; Kwok, K.; Mak, C.; Niu, J.; Zhang, L. Evaluation of pedestrian wind comfort near 'lift-up' buildings with different aspect ratios and central core modifications. *Building and Environment*, 124 (2017), pp. 245-257.